

# Dynamic Structure Factors in Two Dimensional $Z_2$ Lattice Gauge Theory

Firat Yilmaz and Erich J Mueller\*

Laboratory of Atomic and Solid State Physics, Cornell University, Ithaca, New York

(Dated: August 27, 2024)

We numerically calculate the dynamic structure factor of the simplest two dimensional  $Z_2$  lattice gauge theory. This provides an important benchmark for future experiments which will explore the dynamics of such models. As would be expected, the spectrum is gapped away from the critical point, and can be understood in terms of the elementary excitations.

## I. INTRODUCTION

Lattice gauge theories have become an important target for quantum simulation [1–4]. Such simulations would be used for two parallel and interrelated research goals: Modeling the central phenomena in particle physics and exploring the emergent physics of constrained quantum systems [5, 6]. Due to the challenges of numerically studying time dependent quantum mechanical many-body problems, analog simulations are particularly appealing for the insight they give into dynamics. We can use quantum Monte Carlo of lattice QCD to calculate Hadron masses [7], but we cannot use quantum Monte Carlo to directly reproduce a collision experiment. To provide a benchmark for these experiments, we numerically study the dynamic structure factor of the simplest pure  $Z_2$  lattice gauge theory in two dimensions.

In a Lagrangian framework, lattice gauge theories are formulated as models where “matter” degrees of freedom sit on space-time lattice sites, while “gauge” degrees of freedom sit on links [8]. The link variables act as *connections*, relating the local Hilbert space at separate lattice points. This description of the system has a built-in redundancy, as the action is chosen to be invariant under simultaneously applying a rotation to an individual site, and the links connected to it. These rotations form a group, in our case  $Z_2$ . We will work with a *pure* gauge theory, where there are no matter particles. This is analogous to studying electromagnetism in the absence of charges, and we are effectively studying the  $Z_2$  analog of light. Unlike electromagnetism, our gauge excitations are strongly interacting, and have a gapped spectrum.

One dimensional lattice gauge theories have been studied using superconducting circuits [9–16] and cold atoms [17–25]. A number of proposals have emerged for scaling these up to higher dimension [26]. There are exciting ideas about implementing Lorentz symmetry [27], and producing analogs of quantum electrodynamics or quantum chromodynamics [28]. These experiments are typically well suited to exploring dynamics, such as the ones studied here.

Quantum simulations are generally divided into two classes: Digital approaches use a sequence of gates to mimic the Trotterized time evolution [2, 29–32], while

analog approaches directly implement the desired Hamiltonian [33, 34]. The gauge constraints can be implemented by carefully fine-tuning the parameters, or the geometry can be chosen so that they are automatically obeyed. For example, the constrained dynamics in many Rydberg atom experiments [20, 21, 35, 36] are equivalent to lattice gauge theories [37–40]. Tilted lattices lead to similar constraints [41, 42]. Additionally, one can implement models with emergent low energy gauge theory descriptions [43, 44]. There are also a rich set of experiments where density dependent hoppings produce Hamiltonians which have some resemblance to gauge theories, even if they may not display the full gauge symmetry [45–51].

The simplest dynamics experiments involve linear response: One excites the system with a weak probe, and then monitors how some physical property evolves [52]. Equivalent information is given by probes such as electron or neutron scattering. By the fluctuation-dissipation theorem, these response functions are encoded in dynamical correlation functions. In a translationally invariant setting these correlation functions can be decomposed into momentum channels and are described as *dynamic structure factors*. We use *exact diagonalization* to calculate the dynamic structure factors of a  $Z_2$  lattice gauge theory on small systems of up to 36 bonds.

In Sec. II and III we describe our model and numerical technique. In Sec. IV we present our numerical results, and connect them to known properties of the model. Section V contains conclusions and gives an experimental outlook.

## II. MODEL

We consider the  $Z_2$  lattice gauge theory introduced by Wegner in 1971 [53]. It is described by a 2D square array, where a 2-level system (quantum spin) sits on each link. The Hamiltonian consists of Pauli  $X$  and  $Z$  operators. Each plaquette term,  $U_p = Z_i Z_j Z_k Z_l$ , involves a product of Pauli  $Z$  operators, with  $i, j, k, l$  labeling the four spins making up the square plaquette  $p$ . It also contains single site Pauli  $X$  terms, and we will write

$$H = -\cos\theta \sum_p U_p - \sin\theta \sum_i X_i. \quad (1)$$

\* em256@cornell.edu

This Hamiltonian commutes with all of the star operators  $W_s = X_i X_j X_k X_l$ , where  $i, j, k, l$  label the four spins contained in the star  $s$ , ie. the four spins on the bonds connected to a single site – see Fig. 1. This can be interpreted as a  $Z_2$  gauge theory in the temporal gauge, where one takes the time-like component of the vector potential to vanish. The star operators are the generators of spatial gauge transformations, and the physical (gauge invariant) states are the eigenstates of  $W_s$  with eigenvalue 1. The operators  $X_i$  play the role of an electric field, while  $U_p$  can be thought of as a magnetic flux.

As a function of  $\theta \in [0, \pi/2]$ , the ground state of Eq. (1) undergoes a phase transition at  $\theta_c = 0.104\pi$  [8, 54]. For  $\theta < \theta_c$  the system is a  $Z_2$  spin liquid, with a 4-fold degeneracy on the torus. This is referred to as a deconfined phase, as the energy associated with a pair of electric defects (ie. locations where  $W_s = -1$ ) is independent of their separation. For  $\theta > \theta_c$  one has a paramagnet. The ground state is non-degenerate on the torus, and electric defects are confined: The energy of a pair of electric defects varies linearly with their separation.

For  $\theta = 0$  the ground states corresponds to that of the Toric Code [55], they are the simultaneous eigenstate of the  $U_p$  and  $W_s$ , all with eigenvalue +1. The excited states of excess energy  $2n$  instead have  $n$  plaquettes for which  $U_p|\psi\rangle = -|\psi\rangle$ . These are highly degenerate, as there are  $\binom{N_p}{n}$  ways of distributing the flipped plaquettes, where  $N_p$  is the number of plaquettes in the system. For small non-zero  $\theta$ , this degeneracy is broken, giving a bandwidth  $\sim \sin(\theta)$ . Periodic boundary conditions force  $n$  to be even.

For  $\theta = \pi/2$  the ground state is a product state, where every spin is a +1 eigenstate of the  $X$  operator, denoted  $|\rightarrow\rangle$ . Excited states are again degenerate: If  $m$  spins are flipped, the excess energy is  $2m$ . The gauge constraint  $W_s = 1$  restricts the allowed configurations of flipped spins. Any allowed spin configuration can be constructed by flipping spins along a sequence of closed paths. This can be accomplished by applying some product of  $U_p$  operators, supplemented by the non-trivial loops, corresponding to chains of  $Z$  operators which trace out a non-contractible path. There are two such topologically nontrivial loops on a torus. If we restrict ourselves to the space of states that can be reached by applying the  $U_p$  to the ground state, then  $m$  must be even and the smallest allowed  $m$  is 4. If  $\theta$  deviates slightly from  $\pi/2$ , then the degeneracies are broken, yielding bands of width  $\sim \cos(\theta)$ .

In thinking about the properties of this model, it is sometimes convenient to perform a duality transformation, introducing dual spins at the center of each plaquette, whose Pauli operators are  $\bar{X}$  and  $\bar{Z}$ . One envisions a canonical transformation which maps  $U_p$  onto  $\bar{X}_p$ . For each operator  $X_i$  which sits between plaquettes  $p$  and  $p'$ , we identify an operator on the dual spins  $\bar{Z}_p \bar{Z}_{p'}$ . The map from  $\{X, Z\} \rightarrow \{\bar{X}, \bar{Z}\}$  can readily be seen to be Canonical, as it maintains the commutation relations. There are half of many dual spins than gauge spins –

which is accounted for by the constraints  $W_s = 1$ . The mapping, however, is non-local, so care must be taken about boundary conditions. Nonetheless, the spin-liquid phase maps onto a paramagnet in the dual basis, where  $\bar{X}_p = 1$ . The paramagnet of gauge spins maps onto a dual spin ferromagnet. The duality transformation on Eq. (1) maps it onto

$$H = -\cos\theta \sum_i \bar{X}_i - \sin\theta \sum_{\langle ij \rangle} \bar{Z}_i \bar{Z}_j \quad (2)$$

which is the transverse-Field Ising model with  $\Gamma = \cos\theta$  and  $J = \sin\theta$ . According to de Jongh and Van Leeuwen [56], the transition in the 2D transverse field Ising model is at  $\Gamma/J = 3.044(2)$ , corresponding to  $\theta = 0.104\pi$ .

### III. METHODS

To study the dynamical properties of Eq. (1), we consider small systems, where we can fully enumerate a basis for the many-body Hilbert space. We write the Hamiltonian as a matrix in this basis, and then numerically calculate the spectrum. Dynamical correlation functions are found by writing the relevant operators as finite dimensional matrices.

The Hilbert space for an array of 36 spins contains nearly  $10^{11}$  states. If these are gauge spins on the edges of a square grid, the gauge constraints reduces this Hilbert space to  $1.3 \times 10^5$  states. If one breaks this down by momentum sector, the largest sector has  $7.3 \times 10^4$  states in it. In our approach these are the largest matrices that we will need to construct or diagonalize. Unfortunately, due to the exponential scaling with system size, it is very challenging to extend this technique to larger systems. As seen in Fig. 1 we work with periodic arrays of plaquettes, oriented with the lattice oriented at  $45^\circ$  with respect to the boundaries. The gauge spins for a  $L_x \times L_y$  square lattice. To construct the Hilbert space we start with a reference state, where every spin is pointing in the  $+X$  direction. We then conduct a breadth-first search where we systematically apply products of the plaquette operators  $U_p$ , adding the new states to our list of Hilbert space states, and building up the matrix elements of  $H$ , stored as a sparse array. Note, this technique only produces one quarter of the entire Hilbert space: There are four distinct sectors, which are connected by acting with topologically non-trivial chains of  $Z$  operators. In the finite size system, the ground state is always in the sector that we explore, and none of our response functions involve operators which take us out of this sector. Thus for this study it would be wasteful to generate the other sectors.

In this basis we construct translation operators  $T_x$  and  $T_y$ , corresponding to shifting the underlying square lattice. For each basis state  $|\psi\rangle$ , we find the sets of states which are formed by applying powers of  $T_x$  and  $T_y$ . From these we construct momentum eigenstates. Each momentum sector is closed under the action of  $H$ , and we

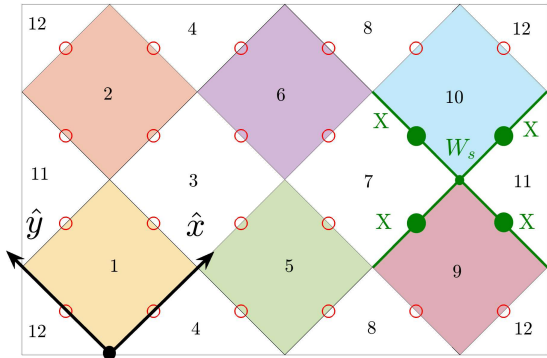


FIG. 1. Gauge spins, marked by red circles, sit on the bonds of a square lattice, oriented  $45^\circ$  with respect to the periodic boundary conditions. We color alternating plaquettes, and number them. The gauge spins form a  $L_x \times L_y$  square lattice. In this case  $L_x = 6$  and  $L_y = 4$ . The plaquette operator  $U_p$  is a product of Pauli  $Z$  operators on the four spins on the edges of the plaquette labeled by the integer  $p$ . The star operators,  $W_s$  correspond to a product of Pauli  $X$  operators on the four spins surrounding a vertex. On the far right of the figure, one example is highlighted. The  $\hat{x}$  and  $\hat{y}$  directions are shown, which are used to define the translation operators  $T_x$  and  $T_y$ .

use a dense matrix eigensolver to separately diagonalize each one. In addition to being numerically efficient, this approach allows us to fix a momentum label to each energy eigenstate. The resulting eigenvalue relation is  $H|\vec{k}, \lambda\rangle = E_\lambda(\vec{k})|\vec{k}, \lambda\rangle$ , where  $\lambda$  is a band index, which labels the different eigenstates. We caution that since we restrict ourselves to one of the four topologically distinct sectors, our spectra will not display the four-fold topological degeneracy that is present in the deconfined phase.

We calculate two dynamical correlation functions

$$S_{XX}(\vec{k}, \omega, \theta) = \langle X_{-\vec{k}}(\omega - H(\theta) + E_0 - i\eta)^{-1} X_{\vec{k}} \rangle_0 \quad (3)$$

$$S_{UU}(\vec{k}, \omega, \theta) = \langle U_{-\vec{k}}(\omega - H(\theta) + E_0 - i\eta)^{-1} U_{\vec{k}} \rangle_0 \quad (4)$$

where  $\eta$  is a small positive number which we use to smooth the spectra. Here

$$X_{\vec{k}} = \sum_j X_j e^{i\vec{k} \cdot \vec{r}_j}, \quad U_{\vec{k}} = \sum_p U_p e^{i\vec{k} \cdot \vec{R}_p}, \quad (5)$$

where  $\vec{r}_j$  is the location of the  $j$ 'th gauge spin and  $\vec{R}_p$  is the center of the plaquette  $p$ . The operators  $X_{\vec{k}}$  and  $U_{\vec{k}}$  connect many-body states with momentum  $\vec{p}$  and  $\vec{p} + \vec{k}$ . We only need to construct the matrix elements between the  $\vec{k} = 0$  sector and  $\vec{k} = \vec{p}$  sector. We then project Eqs (3) and (4) onto the energy eigenstates, reducing it to a series of matrix multiplications. These correlation functions involve gauge invariant quantities. Complementary

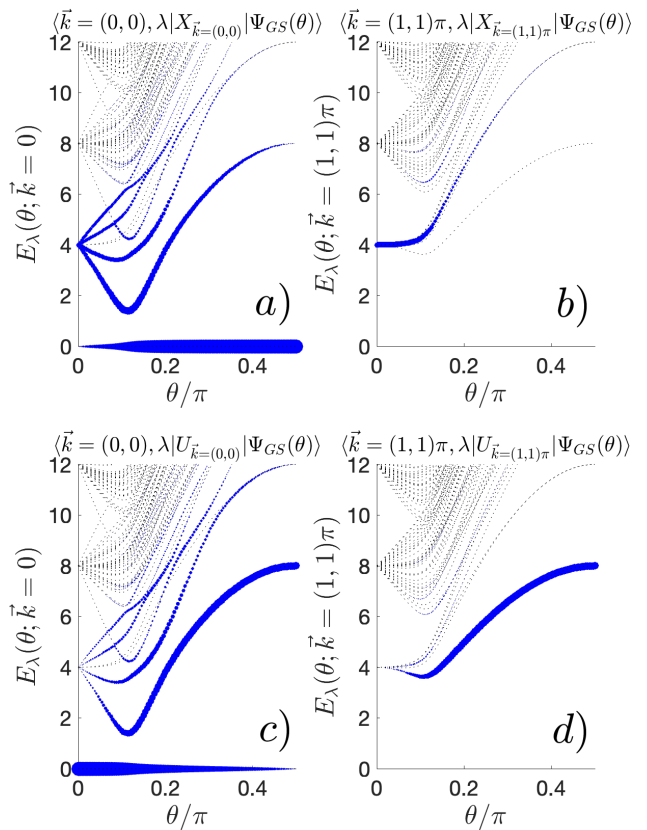


FIG. 2. Spectrum of the  $6 \times 4$  lattice of gauge spins illustrated in Fig. 1, in the fundamental topological sector. Left panels show  $E_\lambda(\vec{k} = (0,0))$ , corresponding to the energies of the states  $|\vec{k} = (0,0), \lambda\rangle$  with  $\vec{k} = (0,0)$ . Here  $\lambda$  indexes the states, and we measure energies relative to the ground state. Blue highlighting indicates the overlaps  $\langle \vec{k}, \lambda | X_{\vec{k}} | \Psi_{GS} \rangle$  (top) or  $\langle \vec{k}, \lambda | U_{\vec{k}} | \Psi_{GS} \rangle$  (bottom). Thicker lines indicate larger overlaps. The right panels show the same quantities but with  $\vec{k} = (1,1)\pi$ .

information can be extracted from spin correlation functions which take one between super-selection sectors [57].

#### IV. RESULTS

Figure 2 shows the spectrum  $E_\lambda(\vec{k})$ , as a function of  $\theta$  for  $\vec{k} = (0,0)$  and  $\vec{k} = (1,1)\pi$  – taking the  $6 \times 4$  lattice of gauge spins illustrated in Fig. 1. Only a single topological sector is shown. For this lattice there are a total of 12 distinct  $k$  points in the first Brillouin zone, but we only show two of them.

At  $\theta = 0$  the energies form degenerate bands with  $E = 2n$  for even integer  $n$ . As discussed in Sec. II, these bands are associated with states with  $n$  flipped plaquettes. Even when we restrict the total momentum of the

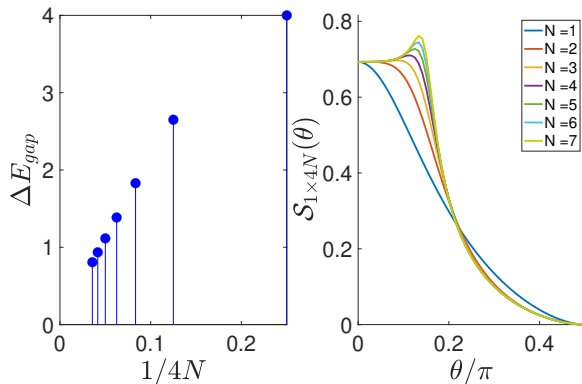


FIG. 3. a) The smallest energy gap,  $\min_{\theta} E(\theta) - E_0$  for a  $2N \times 2$  spin lattice as a function of  $1/N$  where  $N \in 1, 2, \dots, 7$ . It vanishes in the thermodynamic limit, indicating that there is a gapless point. b) The entanglement entropy,  $S(\theta)$  as a function of  $\theta$ , when the  $2N \times 2$  lattice is split into two  $N \times 2$  regions.

state there is a degeneracy, as one can change the relative momenta of the defects. As one increases  $\theta$  the states disperse and the gap  $\Delta(\theta)$  between the ground state and the first excited state initially shrinks. It reaches a minimum near  $\theta = 0.11\pi$ , before growing to  $\Delta(\pi) = 8$ . The states at  $\theta = \pi$  correspond to individual flipped spins, and for a fixed  $\vec{k}$  are non-degenerate.

The minimum in  $\Delta$  is indicative of the phase transition which occurs in the thermodynamic limit. In Fig. 3a we explore this feature by plotting the minimal gap as a function of system size for a ladder geometry of  $N \times 2$  sites. The gap clearly vanishes in the thermodynamic limit. The phase transition can be characterized by a logarithmically divergent entanglement entropy,

$$S(\theta) = -\frac{1}{4N} \text{Tr} \rho_L \log \rho_L, \quad \rho_L = \text{Tr}_R |\Psi_0(\theta)\rangle \langle \Psi_0(\theta)|. \quad (6)$$

Here  $\rho_L$  is the density matrix of the left half of the system, after tracing over the right half. Figure 3b shows the ground state entanglement entropy for ladders of different length. For this geometry at  $\theta = 0$  there is one bit of information shared between the two sides of the system, and hence  $S(0) = \log(2)$ . At  $\theta = \pi$  we have a product state and  $S(\pi) = 0$ . The peak near  $\theta = 0.11\pi$  grows with  $N$ .

In addition to showing the many-body spectrum, Fig. 2 shows the matrix elements,  $\langle \vec{k}, \lambda | X_{\vec{k}} | \Psi_{\text{GS}} \rangle$  and  $\langle \vec{k}, \lambda | U_{\vec{k}} | \Psi_{\text{GS}} \rangle$ , as blue lines whose thickness is proportional to the matrix elements. The operator  $X$  flips a single spin (in the  $\hat{z}$  basis). At small  $\theta$ , this corresponds to flipping two plaquettes, and the bulk of the spectral weight is in the first excited band. For  $\theta$  near  $\pi/2$  the ground state is an eigenstate of  $X$ , and the only matrix element is with the ground state. We can make a similar argument with  $U$ . For small  $\theta$  the ground state is an eigenstate of  $U$ . For  $\theta$  near  $\pi/2$ , the  $U$  operator flips 4

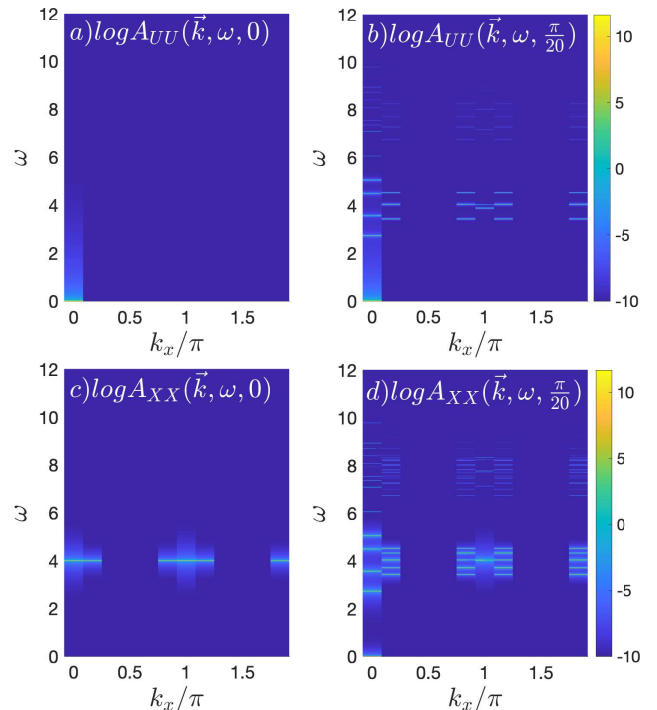


FIG. 4. The deconfined phase logarithm of spectral density plots for the dynamical plaquette-plaquette and bond-bond correlation functions,  $A_{UU}(\vec{k}, \omega, \theta)$ ,  $A_{XX}(\vec{k}, \omega, \theta)$ , respectively. The x-axis corresponds to the x-component of the momentum of the sector: For the 6 geometry shown here,  $k_y = k_x + \pi$  is uniquely determined by  $k_x$ . The y-axis is for the energy,  $\omega$ .

$x$ -spins and the majority of the spectral weight is in the first excited band.

Further details about this structure is conveyed by plotting the spectral densities  $A_X = \text{Im} S_{XX}$  and  $A_U = \text{Im} S_{UU}$ , as shown in Figs. 4 and 5. For our  $6 \times 4$  lattice, the allowed wave-vectors are  $k_x = k_y$  for  $k_x = (2n)\pi/3$  and  $k_x = k_y \pm \pi$  for  $k_x = (2n+1)\pi/6$  where  $n = 0, 1, \dots, 5$ . The momentum sectors are uniquely label by only the  $k_x$  components and we use this choice. At  $\theta = 0$  the  $U$  spectral density in Figs. 4a) is proportional to a delta-function at  $\vec{k} = (0, 0)$  and  $\omega = 0$ . Increasing  $\theta$  to  $\pi/20$ , in panel b) one sees a sequence of peaks appear near  $\omega = 4$ . These peaks are nearly dispersionless: The peak locations are identical at all  $k_x \neq 0, \pi$ . This feature persists to larger  $\theta$ , as shown in 4 a) and b). At  $\theta = \pi/2$  the spectral weight at  $\omega = 0$  vanishes, and the  $U$  spectral density vanishes away from  $\omega = 8$ .

As expected from our previous arguments, the  $X$  spectral weight at  $\theta = 0$  in Fig. 4 c) is found only at  $\omega = 4$ , and is dispersionless. At  $\theta = \pi/20$ , in panel d), the peaks split, but again the frequencies are identical for all  $k_x$  except for  $0, \pi$ . In Fig. 5 c) we see that the  $X$  spectral weight shifts to  $\omega = 0$ ,  $\vec{k} = (0, 0)$  as  $\theta \rightarrow \pi/2$ .

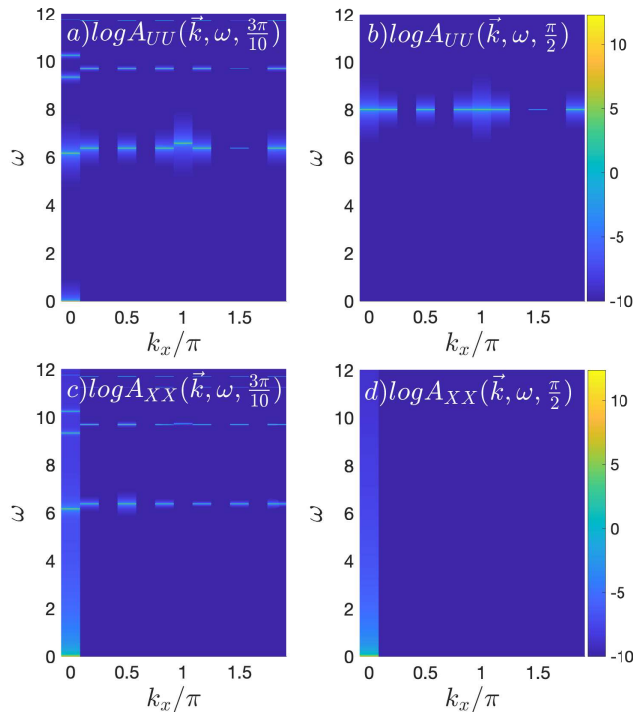


FIG. 5. The confined phase logarithm of spectral density plots for the dynamical plaquette-plaquette and bond-bond correlation functions,  $A_{UU}(\vec{k}, \omega, \theta)$ ,  $A_{XX}(\vec{k}, \omega, \theta)$ , respectively. The x-axis is allocated for lattice momentum sectors (plotted only for  $k_x$ , yet all of  $k_x$  values are unique for our finite size system) and the y-axis is for the energy,  $\omega$ .

## V. CONCLUSION AND EXPERIMENTAL OUTLOOK

Dynamics experiments represent the most important application of lattice gauge theory simulators. Here we calculate the gauge invariant dynamic structure factors associated with the pure  $Z_2$  lattice gauge theory. Far from the phase transition between the confined and deconfined phase we find these response functions can be simply understood in terms of the model's quasiparticles.

These correlation functions can be studied in a number of systems, including cold atoms, Rydberg atoms, and superconducting circuits. The most challenging aspect of cold atom implementations of the Hamiltonian in Eq. 1 is the ring exchange term  $U_p = Z_i Z_j Z_k Z_l$ . There are, however, a number of strategies which have been proposed, typically involving high order perturbation theory

[58]. Constructing this term is simpler in superconducting circuits [59], where one Trotterizes the dynamics, and directly implements gates of the form  $e^{-i(Z_i Z_j Z_k Z_l)\delta t}$ . As illustrated in Fig. 6, this gate can be implemented by introducing a single ancillary qubit for each plaquette. One initializes the auxiliary qubit 0 in state 0. One then applies the gates  $R = CX_{i0}CX_{j0}CX_{k0}CX_{l0}$ , where  $CX_{ij}$  is a control-X operation which flips qubit  $j$  if and

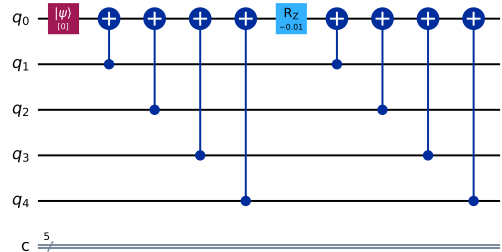


FIG. 6. The Trotterized circuit diagram of the plaquette operator for  $e^{-i(Z_1 Z_2 Z_3 Z_4)\delta t}$  where  $\delta t$  is set to a small number, 0.01. Initially, the ancilla qubit, 0, is set to state 0. One then applies  $R = CX_{i0}CX_{j0}CX_{k0}CX_{l0}$  where  $CX_{ij}$  is a control-X gate which flips qubit  $j$  if and only if  $i$  is in the state 1. One then applies a phase gate to the ancilla qubit  $e^{-iZ_0\delta t}$ , shown as a light blue box. The desired Trotterized operator is generated by applying  $R$  once again,  $Re^{-iZ_0\delta t}R = e^{-i(Z_1 Z_2 Z_3 Z_4)\delta t}$ .

only if  $i$  is in the excited state. The operation  $U$  entangles the ancilla with the plaquette. A phase gate is applied to the ancilla,  $e^{iZ_0\phi}$ . One once again applies  $U$ . Straightforward arithmetic gives  $Re^{iZ_0\phi}R = e^{iZ_0Z_1Z_2Z_3Z_4\phi}$ , which is the desired evolution operator when acting on an eigenstate of  $Z_0$ .

The response functions are most easily measured in the temporal domain. For example, at time  $t = 0$  one applies a  $U$  or  $X$  gate. At a later time  $t$  one measures either  $U$  or  $X$ . The expectation value of that measurement is exactly  $S_{XX}(t)$  or  $S_{UU}(t)$ .

## VI. ACKNOWLEDGEMENTS

F.Y. is supported by the Deutsche Forschungsgemeinschaft (DFG, German Research Foundation) through project TRR360 A5 and Türkiye Bilimsel ve Teknolojik Araştırma Kurumu (TÜBİTAK) call no.2219. EJM acknowledges support from NSF PHY-2409403.

[1] J. C. Halimeh, M. Aidelsburger, F. Grusdt, P. Hauke, and B. Yang, Cold-atom quantum simulators of gauge theories (2023), arXiv:2310.12201 [cond-mat.quant-gas].

[2] C. W. Bauer, Z. Davoudi, A. B. Balantekin, T. Bhattacharya, M. Carena, W. A. de Jong, P. Draper, A. El-Khadra, N. Gemelke, M. Hanada, D. Kharzeev, H. Lamm, Y.-Y. Li, J. Liu, M. Lukin, Y. Meurice,

- C. Monroe, B. Nachman, G. Pagano, J. Preskill, E. Rinaldi, A. Roggero, D. I. Santiago, M. J. Savage, I. Siddiqi, G. Siopsis, D. Van Zanten, N. Wiebe, Y. Yamauchi, K. Yeter-Aydeniz, and S. Zorzetti, Quantum simulation for high-energy physics, PRX Quantum **4**, 027001 (2023).
- [3] M. Dalmonte and S. Montangero, Lattice gauge theory simulations in the quantum information era, Contemporary Physics **57**, 388–412 (2016).
- [4] U. Wiese, Ultracold quantum gases and lattice systems: Quantum simulation of lattice gauge theories, Annalen der Physik **525**, 777–796 (2013).
- [5] T. Senthil and M. P. A. Fisher,  $Z_2$  gauge theory of electron fractionalization in strongly correlated systems, Phys. Rev. B **62**, 7850 (2000).
- [6] P. E. Lammert, D. S. Rokhsar, and J. Toner, Topology and nematic ordering. i. A gauge theory, Phys. Rev. E **52**, 1778 (1995).
- [7] S. Muroya, A. Nakamura, C. Nonaka, and T. Takaishi, Lattice QCD at finite density: An introductory review, Progress of Theoretical Physics **110**, 615 (2003).
- [8] J. B. Kogut, An introduction to lattice gauge theory and spin systems, Reviews of Modern Physics **51**, 659 (1979).
- [9] E. A. Martinez, C. A. Muschik, P. Schindler, D. Nigg, A. Erhard, M. Heyl, P. Hauke, M. Dalmonte, T. Monz, P. Zoller, and R. Blatt, Real-time dynamics of lattice gauge theories with a few-qubit quantum computer, Nature **534**, 516 (2016).
- [10] C. Kokail, C. Maier, R. van Bijnen, T. Brydges, M. K. Joshi, P. Jurcevic, C. A. Muschik, P. Silvi, R. Blatt, C. F. Roos, and P. Zoller, Self-verifying variational quantum simulation of lattice models, Nature **569**, 355 (2019).
- [11] N. Mueller, J. A. Carolan, A. Connelly, Z. Davoudi, E. F. Dumitrescu, and K. Yeter-Aydeniz, Quantum computation of dynamical quantum phase transitions and entanglement tomography in a lattice gauge theory, PRX Quantum **4**, 030323 (2023).
- [12] N. Klco, E. F. Dumitrescu, A. J. McCaskey, T. D. Morris, R. C. Pooser, M. Sanz, E. Solano, P. Lougovski, and M. J. Savage, Quantum-classical computation of Schwinger model dynamics using quantum computers, Phys. Rev. A **98**, 032331 (2018).
- [13] Z. Wang, Z.-Y. Ge, Z. Xiang, X. Song, R.-Z. Huang, P. Song, X.-Y. Guo, L. Su, K. Xu, D. Zheng, and H. Fan, Observation of emergent  $Z_2$  gauge invariance in a superconducting circuit, Phys. Rev. Res. **4**, L022060 (2022).
- [14] J. Mildenerberger, W. Mruczkiewicz, J. C. Halimeh, Z. Jiang, and P. Hauke, Probing confinement in a  $Z_2$  lattice gauge theory on a quantum platform, arXiv:2203.08905 [quant-ph] (2022), arXiv:2203.08905 [quant-ph].
- [15] E. Huffman, M. García Vera, and D. Banerjee, Toward the real-time evolution of gauge-invariant  $Z_2$  and  $u(1)$  quantum link models on noisy intermediate-scale quantum hardware with error mitigation, Phys. Rev. D **106**, 094502 (2022).
- [16] G. Pardo, T. Greenberg, A. Fortinsky, N. Katz, and E. Zohar, Resource-efficient quantum simulation of lattice gauge theories in arbitrary dimensions: Solving for Gauss’s law and fermion elimination, Phys. Rev. Res. **5**, 023077 (2023).
- [17] C. Schweizer, F. Grusdt, M. Berngruber, L. Barbiero, E. Demler, N. Goldman, I. Bloch, and M. Aidelsburger, Floquet approach to  $Z_2$  lattice gauge theories with ultracold atoms in optical lattices, Nature Physics **15**, 1168 (2019).
- [18] A. Mil, T. V. Zache, A. Hegde, A. Xia, R. P. Bhatt, M. K. Oberthaler, P. Hauke, J. Berges, and F. Jendrzejewski, A scalable realization of local  $U(1)$  gauge invariance in cold atomic mixtures, Science **367**, 1128 (2020).
- [19] A. Frölian, C. S. Chisholm, E. Neri, C. R. Cabrera, R. Ramos, A. Celi, and L. Tarruell, Realizing a 1D topological gauge theory in an optically dressed BEC, Nature **608**, 293 (2022).
- [20] H. Bernien, S. Schwartz, A. Keesling, H. Levine, A. Omran, H. Pichler, S. Choi, A. S. Zibrov, M. Endres, M. Greiner, *et al.*, Probing many-body dynamics on a 51-atom quantum simulator, Nature **551**, 579 (2017).
- [21] B. Yang, H. Sun, R. Ott, H.-Y. Wang, T. V. Zache, J. C. Halimeh, Z.-S. Yuan, P. Hauke, and J.-W. Pan, Observation of gauge invariance in a 71-site Bose-Hubbard quantum simulator, Nature **587**, 392 (2020).
- [22] Z.-Y. Zhou, G.-X. Su, J. C. Halimeh, R. Ott, H. Sun, P. Hauke, B. Yang, Z.-S. Yuan, J. Berges, and J.-W. Pan, Thermalization dynamics of a gauge theory on a quantum simulator, Science **377**, 311 (2022).
- [23] H.-Y. Wang, W.-Y. Zhang, Z. Yao, Y. Liu, Z.-H. Zhu, Y.-G. Zheng, X.-K. Wang, H. Zhai, Z.-S. Yuan, and J.-W. Pan, Interrelated thermalization and quantum criticality in a lattice gauge simulator, Physical Review Letters **131**, 10.1103/physrevlett.131.050401 (2023).
- [24] W.-Y. Zhang, Y. Liu, Y. Cheng, M.-G. He, H.-Y. Wang, T.-Y. Wang, Z.-H. Zhu, G.-X. Su, Z.-Y. Zhou, Y.-G. Zheng, H. Sun, B. Yang, P. Hauke, W. Zheng, J. C. Halimeh, Z.-S. Yuan, and J.-W. Pan, Observation of microscopic confinement dynamics by a tunable topological quantum simulator, arXiv:2306.11794 [cond-mat.quant-gas] (2023), arXiv:2306.11794 [cond-mat.quant-gas].
- [25] H.-Y. Wang, W.-Y. Zhang, Z. Yao, Y. Liu, Z.-H. Zhu, Y.-G. Zheng, X.-K. Wang, H. Zhai, Z.-S. Yuan, and J.-W. Pan, Interrelated thermalization and quantum criticality in a lattice gauge simulator, Physical Review Letters **131**, 050401 (2023).
- [26] E. Zohar, A. Farace, B. Reznik, and J. I. Cirac, Digital quantum simulation of  $Z_2$  lattice gauge theories with dynamical fermionic matter, Phys. Rev. Lett. **118**, 070501 (2017).
- [27] T. V. Zache, F. Hebenstreit, F. Jendrzejewski, M. K. Oberthaler, J. Berges, and P. Hauke, Quantum simulation of lattice gauge theories using Wilson fermions, Quantum Science and Technology **3**, 034010 (2018).
- [28] E. Kapit and E. Mueller, Optical-lattice Hamiltonians for relativistic quantum electrodynamics, Phys. Rev. A **83**, 033625 (2011).
- [29] L. Tagliacozzo, A. Celi, A. Zamora, and M. Lewenstein, Optical Abelian lattice gauge theories, Annals of Physics **330**, 160–191 (2013).
- [30] L. Tagliacozzo, A. Celi, P. Orland, M. W. Mitchell, and M. Lewenstein, Simulation of non-Abelian gauge theories with optical lattices, Nature Communications **4**, 10.1038/ncomms3615 (2013).
- [31] E. Zohar, A. Farace, B. Reznik, and J. I. Cirac, Digital lattice gauge theories, Phys. Rev. A **95**, 023604 (2017).
- [32] J. Bender, E. Zohar, A. Farace, and J. I. Cirac, Digital quantum simulation of lattice gauge theories in three spatial dimensions, New Journal of Physics **20**, 093001 (2018).
- [33] M. Aidelsburger, L. Barbiero, A. Bermudez, T. Chanda, A. Dauphin, D. González-Cuadra, P. R. Grzy-

- bowski, S. Hands, F. Jendrzejewski, J. Jünemann, *et al.*, Cold atoms meet lattice gauge theory, *Philosophical Transactions of the Royal Society A* **380**, 20210064N (2022).
- [34] L. Barbiero, C. Schweizer, M. Aidelsburger, E. Demler, N. Goldman, and F. Grusdt, Coupling ultracold matter to dynamical gauge fields in optical lattices: From flux attachment to  $Z_2$  lattice gauge theories, *Science Advances* **5**, 10.1126/sciadv.aav7444 (2019).
- [35] G. Semeghini, H. Levine, A. Keesling, S. Ebadi, T. T. Wang, D. Bluvstein, R. Verresen, H. Pichler, M. Kalinowski, R. Samajdar, A. Omran, S. Sachdev, A. Vishwanath, M. Greiner, V. Vuletić, and M. D. Lukin, Probing topological spin liquids on a programmable quantum simulator, *Science* **374**, 1242–1247 (2021).
- [36] S. Ebadi, T. T. Wang, H. Levine, A. Keesling, G. Semeghini, A. Omran, D. Bluvstein, R. Samajdar, H. Pichler, W. W. Ho, *et al.*, Quantum phases of matter on a 256-atom programmable quantum simulator, *Nature* **595**, 227 (2021).
- [37] F. M. Surace, P. P. Mazza, G. Giudici, A. Lerose, A. Gambassi, and M. Dalmonte, Lattice gauge theories and string dynamics in Rydberg atom quantum simulators, *Physical Review X* **10**, 021041 (2020).
- [38] Y. Cheng and C. Li, Gauge theory description of Rydberg atom arrays with a tunable blockade radius, *Physical Review B* **107**, 094302 (2023).
- [39] J. Zhang, J. Unmuth-Yockey, J. Zeiher, A. Bazavov, S.-W. Tsai, and Y. Meurice, Quantum simulation of the universal features of the Polyakov loop, *Physical Review Letters* **121**, 223201 (2018).
- [40] A. Celi, B. Vermersch, O. Viyuela, H. Pichler, M. D. Lukin, and P. Zoller, Emerging two-dimensional gauge theories in Rydberg configurable arrays, *Physical Review X* **10**, 021057 (2020).
- [41] S. Sachdev, K. Sengupta, and S. M. Girvin, Mott insulators in strong electric fields, *Phys. Rev. B* **66**, 075128 (2002).
- [42] S. Pielawa, T. Kitagawa, E. Berg, and S. Sachdev, Correlated phases of bosons in tilted frustrated lattices, *Phys. Rev. B* **83**, 205135 (2011).
- [43] E. Zohar, J. I. Cirac, and B. Reznik, Quantum simulations of lattice gauge theories using ultracold atoms in optical lattices, *Reports on Progress in Physics* **79**, 014401 (2015).
- [44] R. Samajdar, D. G. Joshi, Y. Teng, and S. Sachdev, Emergent  $Z_2$  gauge theories and topological excitations in Rydberg atom arrays, *Phys. Rev. Lett.* **130**, 043601 (2023).
- [45] F. Görg, K. Sandholzer, J. Minguzzi, R. Desbuquois, M. Messer, and T. Esslinger, Realization of density-dependent Peierls phases to engineer quantized gauge fields coupled to ultracold matter, *Nature Physics* **15**, 1161 (2019).
- [46] T. Keilmann, S. Lanzmich, I. McCulloch, and M. Roncaglia, Statistically induced phase transitions and anyons in 1d optical lattices, *Nature Communications* **2**, 10.1038/ncomms1353 (2011).
- [47] S. Greschner, G. Sun, D. Poletti, and L. Santos, Density-dependent synthetic gauge fields using periodically modulated interactions, *Phys. Rev. Lett.* **113**, 215303 (2014).
- [48] S. Greschner and L. Santos, Anyon Hubbard model in one-dimensional optical lattices, *Phys. Rev. Lett.* **115**, 053002 (2015).
- [49] A. Bermudez and D. Porras, Interaction-dependent photon-assisted tunneling in optical lattices: a quantum simulator of strongly-correlated electrons and dynamical gauge fields, *New Journal of Physics* **17**, 103021 (2015).
- [50] C. Sträter, S. C. L. Srivastava, and A. Eckardt, Floquet realization and signatures of one-dimensional anyons in an optical lattice, *Phys. Rev. Lett.* **117**, 205303 (2016).
- [51] L. W. Clark, B. M. Anderson, L. Feng, A. Gaj, K. Levin, and C. Chin, Observation of density-dependent gauge fields in a Bose-Einstein condensate based on micro-motion control in a shaken two-dimensional lattice, *Phys. Rev. Lett.* **121**, 030402 (2018).
- [52] G. D. Mahan, *Many-particle physics* (Springer Science & Business Media, 2013).
- [53] F. J. Wegner, Duality in generalized Ising models and phase transitions without local order parameters, *Journal of Mathematical Physics* **12**, 2259 (1971).
- [54] U. Borla, B. Jeevanesan, F. Pollmann, and S. Moroz, Quantum phases of two-dimensional  $Z_2$  gauge theory coupled to single-component fermion matter, *Phys. Rev. B* **105**, 075132 (2022).
- [55] A. Y. Kitaev, Fault-tolerant quantum computation by anyons, *Annals of physics* **303**, 2 (2003).
- [56] M. d. C. de Jongh and J. Van Leeuwen, Critical behavior of the two-dimensional Ising model in a transverse field: A density-matrix renormalization calculation, *Physical Review B* **57**, 8494 (1998).
- [57] H.-Y. Qi and W. Zheng, Gauge violation spectroscopy of synthetic gauge theories, *Phys. Rev. Res.* **6**, 013047 (2024).
- [58] O. I. Motrunich, Orbital magnetic field effects in spin liquid with spinon Fermi sea: Possible application to  $\kappa$ -(ET) $_2$ Cu $_2$ (CN) $_3$ , *Physical Review B—Condensed Matter and Materials Physics* **73**, 154407 (2006).
- [59] R. Irmejs, M.-C. Bañuls, and J. I. Cirac, Quantum simulation of  $Z_2$  lattice gauge theory with minimal resources, *Physical Review D* **108**, 074503 (2023).